Elsayed, Sherif; Hummel, Michael; Sawada, Daisuke; Guizani, Chamseddine; Rissanen, Marja; Sixta, Herbert

Superbase-based protic ionic liquids for cellulose filament spinning

Published in:
Cellulose

DOI:
10.1007/s10570-020-03505-y

Published: 01/01/2021

Document Version
Publisher's PDF, also known as Version of record

Cellulose
https://doi.org/10.1007/s10570-020-03505-y

ORIGINAL RESEARCH

Superbase-based protic ionic liquids for cellulose filament spinning

Sherif Elsayed · Michael Hummel · Daisuke Sawada · Chamseddine Guizani · Marja Rissanen · Herbert Sixta

Received: 14 July 2020 / Accepted: 1 October 2020

Abstract Lyocell fibers have received increased attention during the recent years. This is due to their high potential to satisfy the rising market demand for cellulose-based textiles in a sustainable way. Typically, this technology adopts a dry-jet wet spinning process, which offers regenerated cellulose fibers of excellent mechanical properties. Compared to the widely exploited viscose process, the lyocell technology fosters an eco-friendly process employing green direct solvents that can be fully recovered with low environmental impact. *N*-methylmorpholine *N*-oxide (NMMO) is a widely known direct solvent that has proven its success in commercializing the lyocell process. Its regenerated cellulose fibers exhibit higher tenacities and chain orientation compared to viscose fibers. Recently, protic superbase-based ionic liquids (ILs) have also been found to be suitable solvents for lyocell-type fiber spinning. Similar to NMMO, fibers of high mechanical properties can be spun from the cellulose-IL solutions at lower spinning temperatures. In this article, we study the different aspects of producing regenerated cellulose fibers using NMMO and relevant superbase-based ILs. The selected ILs are 1,5-diazabicyclo[4.3.0]non-5-ene-1-ium acetate ([DBNH]OAc), 7-methyl-1,5,7-triazabicyclo[4.4.0]dec-5-enium acetate ([mTBDH]OAc) and 1,8-diazabicyclo[5.4.0]undec-7-enium acetate ([DBU-H]OAc). All ILs were used to dissolve a 13 wt% (PHK) cellulose pulp. The study covers the fiber spinning process, including the rheological characterization of the various cellulose solutions. Moreover, we discuss the properties of the produced fibers such as mechanical performance, macromolecular properties and morphology.

Electronic supplementary material The online version of this article (https://doi.org/10.1007/s10570-020-03505-y) contains supplementary material, which is available to authorized users.

S. Elsayed · M. Hummel · D. Sawada · C. Guizani · M. Rissanen · H. Sixta (✉)
Department of Bioproducts and Biosystems, Aalto University, P.O. Box 16300, 00076 Aalto, Finland
e-mail: herbert.sixta@aalto.fi

S. Elsayed
e-mail: sherif.elsayed@aalto.fi

M. Hummel
e-mail: michael.hummel@aalto.fi

D. Sawada
e-mail: daisuke.sawada@aalto.fi

C. Guizani
e-mail: chamseddine.guizani@aalto.fi

M. Rissanen
e-mail: marja.rissanen@aalto.fi

Published online: 20 October 2020

Graphic abstract

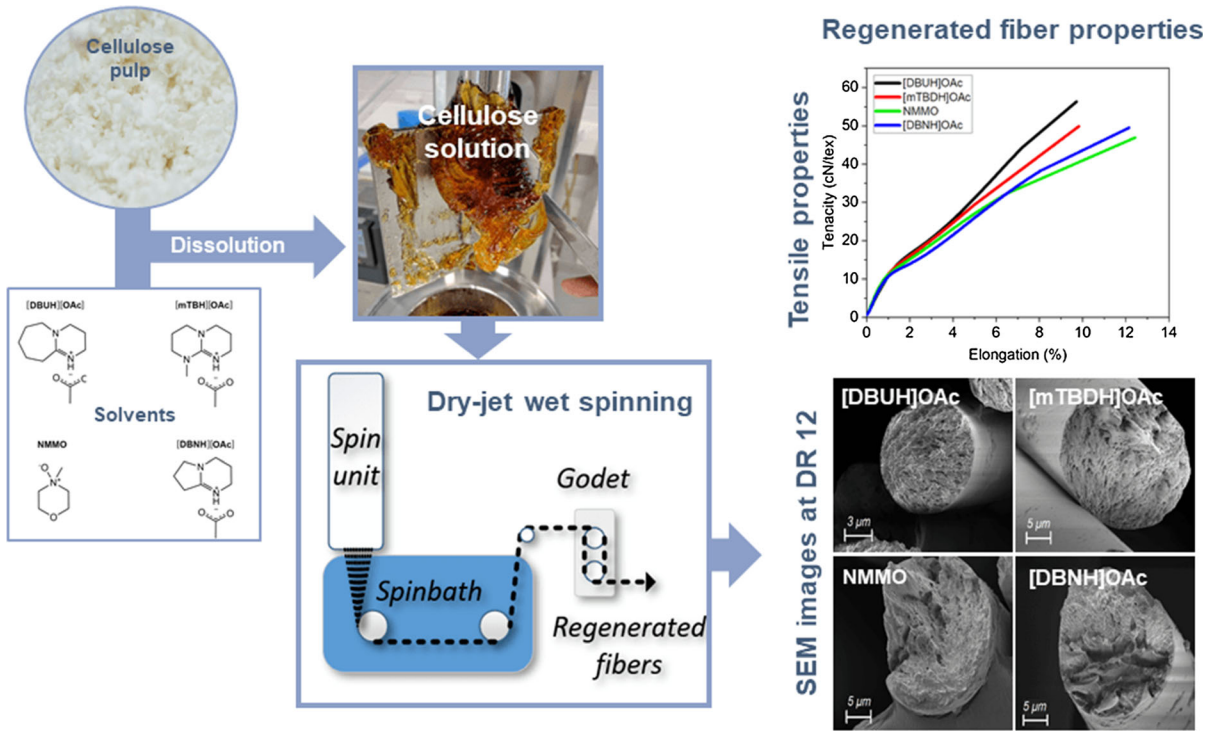

Keywords Lyocell · Regenerated fibers · MMCFs · Ionic liquids · Cellulose dissolution · Ioncell

Introduction

Cellulosic fibers long dominated the man-made fiber market until the synthetic fiber production surpassed cellulosics in the late 1960s (The Fiber Year 2013). Ever since, the man-made cellulose fibers have been in the shadow of polyesters, polyamides and acrylics. However, more and more problems are emerging in connection with the ubiquitous use of plastics. For instance, an increasing share of the plastic debris is discharged during laundering and enters the marine environment, where weathering causes fragmentation into so-called secondary microplastics that even small marine invertebrates may ingest (Goldstein and Goodwin 2013). By 2100, a 50-fold increase of buoyant microplastic particles (ca. 50 particles m^{-3}) and ca. 8000 particles kg^{-1} of sedimented microplastic particles are predicted (Everaert et al. 2018). This and other environment and health-threatening issues have led to a renaissance of cellulosic fibers. In 2018, the total man-made cellulosics production was 6.8 million tonnes, with viscose accounting for 5.6 million tonnes (The Fiber Year 2019). The viscose technology, however, is associated with a number of drawbacks and limitations. It consists of a long processing cascade and requires large amounts of CS_2 and caustic, which results in hazardous byproducts such as H_2S gases and other volatile thio-compounds posing severe threats on the environment and work forces. Alternative solutions to satisfy the increasing demand for cellulosic fibers are thus needed. At present, only one lyocell-type fiber has a noteworthy share on the fiber market. Lyocell is a generic name which is derived from the Greek word *lyein* (meaning dissolve) and *cell* from cellulose, and describes a process in which cellulose is dissolved without chemical modification in a direct solvent and spun in a dry-jet wet spinning process via an air gap into an aqueous coagulation bath. Currently, the only commercial lyocell solution is based on the solvent *N*-methylmorpholine *N*-oxide (NMMO) monohydrate. With the development starting as early as in the late 1960s, the first commercial production plant started operation in the early 1990s.

In 2018, this fiber type, sold under the trademark Tencel, had a market volume of ca. 220,000 annual tones with another 100,000 tonnes plant being built. The continuous expansion of the global lyocell capacity reflects the increasing demand for sustainably produced bio-based fibers. This and certain stability issues associated with NMMO (Buijtenhuijs et al. 1986; Rosenau et al. 2001; Jusner et al. 2020), have motivated research on other cellulose solvents that allow for direct dissolution and subsequent fiber spinning. Meanwhile, a wide spectrum of cellulose solvent systems is known, including electrolyte solutions [DMAc/LiCl (Hansen and Björkman 1998), DMSO/TBAF (Heinze et al. 2000; Köhler and Heinze 2007), ammonia or amine/thiocyanate (Hattori et al. 2002, 2004), [BMIM]Cl/DMI (Rinaldi 2011)], phosphoric acids (Bredereck and Hermanutz 2005; Liebert 2010), metal complex-based solvents (Horvath 2006; Liebert 2010), and aqueous sodium hydroxide (with and without additives) (Budtova and Navard 2016; Kamida et al. 1984; Kamide et al. 1992; Yamashiki et al. 1992). However, all of them suffer from certain problems and shortcomings which have yet prevented them from scaling-up to commercially relevant levels.

Strictly speaking, this also applies to ionic liquids (ILs) which are the subject of the article at hand. Although ILs have been described already at the beginning of the 20th century (Walden 1914), notable research activities in this field emerged only in the 1990s. The definition of ILs and a comprehensive overview can be found in the seminal review by Welton (1999). At the beginning of the 21st century, ILs were found to dissolve biopolymers such as cellulose, but also secondary wood polymers (hemicellulose, lignin) and wood in its entirety. For details, the reader is referred to a set of earlier published reviews (Brandt et al. 2013; Lê et al. 2019; Maeki-Arvela et al. 2010; Pinkert et al. 2009; Singh and Simmons 2013; Wang et al. 2012). Notably, most of the described biomass-dissolving ILs were imidazolium-based and only very few comprised other heterocycles such as 1-alkylpyridinium, 1-alkyl-1-methylpyrrolidinium, and guanidinium or non-cyclic quaternary cations like tetraalkylammonium and phosphonium ions (El Seoud et al. 2007; Laus et al. 2005; Maeki-Arvela et al. 2010). Further, they all included an anion with a high hydrogen-bond (net) basicity (Crowhurst et al. 2003; Doherty et al. 2010; Hauru et al. 2012). The most prominent ones regarding cellulose-dissolving ILs are halides (Swatloski et al. 2002), carboxylates (Fukaya et al. 2006), and phosphates (Brandt et al. 2010; Fukaya et al. 2008). Various ILs representing combinations of above mentioned cations and anions have been proposed for spinning of (ligno-)cellulosic filaments. A comprehensive summary of IL-based fiber spinning was given earlier (Hummel et al. 2016). The majority of those studies focus on imidazolium chlorides and acetates. They can dissolve cellulose and other biopolymers in high concentrations, and in particular imidazolium acetate ILs are characterized by low viscosity, facilitating handling and dissolution. Yet, imidazolium-ILs suffer from a number of drawbacks limiting their potential for large-scale fiber spinning. Usually, the halide-containing IL require a comparatively high dissolution and processing temperatures at which the IL can decompose (Kosmulski et al. 2004; Meine et al. 2010), and cellulose polymers are degraded substantially even if stabilizers are added (Bentivoglio et al. 2006; Gazit and Katz 2012; Laus et al. 2005). These problems can be alleviated to some extent when replacing the halide anion with acetate (Michud et al. 2015a). Nonetheless, side reactions induced by the imidazolium moiety such as cellulose modification (Clough et al. 2015; Ebner et al. 2008) and acetylation through trans-acylation may occur (Zweckmair et al. 2015).

Apart from thermal and chemical integrity, the spinning of filaments requires distinct visco-elastic properties of the cellulose-IL solutions. These requirements are less strict for wet spinning where the coagulation of the filaments happens instantly after the solutions exit the spinneret. Hence, no or very limited draw is applied to the filament. Consequently, the total orientation and crystallinity of the resulting fibers are low, resulting in moderate mechanical properties. In contrast, dry-jet wet spinning results in filaments and fibers with a pronounced macromolecular orientation and high mechanical properties. The decisive difference between wet and dry-jet wet spinning is that in the case of the latter the spinneret is outside the spin bath and the visco-elastic filaments pass through an air gap (typically only a few centimeters long) before they immerge into a coagulating medium. By adjusting the filament take-up velocity to a multiple of the linear extrusion velocity, the filaments are stretched predominately in the air gap. Once the filaments get into contact with the spin bath rapid solvent exchange

causes instant coagulation which is believed to follow spinodal decomposition (Nishiyama et al. 2019). The stretch of the filament is called draw and creates a uniaxial stress tensor acting on the polymer chains in solution. The polymers adopt an oriented structure with a predominant direction parallel to the filament axis, which is preserved in the final solid fiber due to the rapid solidification in the spin bath. This axial orientation results in high tensile strength and modulus known for lyocell-type fibers and is usually not accessible through classical wet-spinning processes.

Evidently, the filament draw also reduces the diameter of the final cellulosic fiber. A final fiber diameter of ca. 10–13 µm (correspond to 1–2 dtex) is mandatory for technical applications such as composite reinforcement and in particular to produce yarns for textiles and clothing. Although the reduction of the diameter may seem trivial, it is one of the key issues that disqualifies most cellulose-IL solutions, which lack the necessary viscoelasticity for filament draw. Various breaching mechanisms in the air gap depend on the initial filament diameter, which limits the minimum diameter of the spinneret orifices (Ziabicki and Takserman-Krozer 1964a, b). If the filament is too thin when exiting the spinneret it will breach in the air gap. Thus, the draw-ability of an initially thick filament is a central requirement for dry-jet wet spinning to yield thin and strong fibers. The archetypical IL [emim]OAc does not provide the addressed viscoelasticity and its suitability as solvent for dry-jet wet spinning is thus limited (Hauru et al. 2016).

We found earlier that the amidine-based ionic liquid 1,5-diazabicyclo[4.3.0]non-5-ene-1-ium acetate ([DBNH]OAc) is an excellent solvent to process cellulose in a lyocell-type spin process (Hummel et al. 2016; Michud et al. 2016b; Sixta et al. 2015). It contains acetate as an established anion that provides the necessary hydrogen bond basicity to dissolve cellulose. Obtained through simple mixture of the superbase with equimolar acetic acid, the resulting IL dissolves lignocellulose rapidly at mild processing temperatures ($\leq$ 80 °C). More importantly, the resulting solutions depict visco-elastic properties suitable for dry-jet wet spinning at high draw ratios (up to 20) (Ma et al. 2016a). After studying systematically the influence of the composition (Ma et al. 2016a, b) and molecular weight distribution (Michud et al. 2015b) of the lignocellulosic solute on the spinnability, we now looked at alternative superbase-based ILs: 1,8-Diazabicyclo[5.4.0]undec-7-enium acetate ([DBUH]OAc), an amidine-based IL, and 7-methyl-1,5,7-triazabicyclo[4.4.0]dec-5-enium acetate ([mTBDH]OAc), a guanidine-based IL. Similar to DBN, both DBU and mTBD ILs are capable of dissolving high cellulose contents (Parviainen et al. 2013; Kuzmina et al. 2017; Elsayed et al. 2020). Herein, we report on the suitability of these ILs as spinning solvents and compare their performance with NMMO monohydrate as a benchmark.

Materials and methods

The superbases were received as follows; DBN (Fluorochem, United Kingdom), DBU (Merck, Germany), and mTBD (BOC Sciences, USA). Respective ILs were prepared by the addition of equimolar glacial acetic acid (Merck, Germany) to the superbases (DBN, DBU and mTBD). [emim]OAc was available from Merck, Germany. The IL preparation was carried out in a controlled temperature glass reactor under continuous stirring for 1 h. The reaction temperature was set to 70 °C for the synthesis of [DBNH]OAc and [DBUH]OAc, and 80 °C for the synthesis of [mTBDH]OAc. NMMO monohydrate (Alfa Aesar, Germany) was used as received. Propyl gallate powder (Merck, Germany) and NaOH pellets (VWR, Finland) were used as stabilizers during the NMMO dope preparation. Cellulose pulp sheets, birch prehydrolysis kraft (PHK) (intrinsic viscosity = 494 ml/g, Mw = 160.5 kD_a, polydispersity index 3.6, Pure by Stora Enso, Enocell mill, Finland), was received and ground in a Wiley mill.

Cellulose dissolution took place in a vertical kneader by adding 13 wt% of cellulose (of the total mass) to the ILs and NMMO, respectively. An additional 0.3 wt% (oven-dry mass of pulp) propyl gallate and 0.13 wt% (oven-dry mass of pulp) NaOH were added to the NMMO/pulp mixture prior to mixing. Thereafter, the kneader was closed and let to stir for 90 min with 30 RPM under a vacuum pressure of 20 mbar. The applied temperature was 80 °C for the [DBNH]OAc-cellulose and [emim]OAc-cellulose solutions, 85 °C for [mTBDH]OAc-cellulose solution and 95 °C for [DBUH]OAc and NMMO-cellulose solutions. Following dissolution, the cellulose-IL solutions also referred to as dopes, were filtrated in a hydraulic press system (170 bar, metal filter fleece,

5–6 µm absolute fineness) to remove any undissolved cellulose particles. Finally, the clear solutions were wrapped and sealed against moisture and preserved in cold room storage.

Fiber spinning was performed by the means of a dry-jet wet piston unit (Fourné Polymertechnik, Germany). The dope was fed to the spinning cylinder and extruded through the spinneret capillaries. The filaments were aligned and stretched in an air gap before regenerating in a ca. 110 L water spin bath and finally collected around a spinning godet. The extrusion velocity was 3.5 m/min, whilst the take-up velocity gradually increased from 7 to 42 m/min, i.e., the draw ratio (DR) range of 2–12. The spinneret was of 200 holes, 100 µm capillary diameter and a length-to-diameter ratio of 0.2. The air gap distance was 1 cm and the temperature of the bath was fixed to 12 °C throughout the process. Over the course of the spinning process, different temperatures were employed for the various dopes. The temperatures were ca. 80 °C for the [DBNH]OAc, 85 °C for the [mTBDH]OAc, and 95 °C [DBUH]OAc and NMMO dopes. Directly after spinning, the regenerated filaments were cut into 10 cm fibers and washed at 80 °C for 2 h to rinse off the residual IL. The washing water was changed to fresh water after the first hour interval.

Rheological characterization

The shear rheological properties of the dopes were analyzed with Anton Paar MCR 302 parallel plate device (25 mm plate diameter, 1 mm gap size). Oscillatory measurements followed a similar protocol (strain, angular frequency range, and temperatures) as described in our previous publications (Hummel et al. 2016; Michud et al. 2016a). Using this sequence, it was possible to measure the sample complex viscosity (η^*), storage moduli (G') and the loss moduli (G''). From the data, the zero shear viscosity was extrapolated via fitting η^* to Cross viscosity model as shown in the below equation, where C and p are (cross) time and rate constant respectively.

$$\eta = \frac{\eta_0 - \eta_\infty}{1 + (C\dot{\gamma})^p} + \eta_\infty \quad (1)$$

The master curves for the complex viscosity and the dynamic moduli were derived from the reduced variables via WLF time–temperature superposition. The shift factors and reduced variables were calculated as described by Sammons et al. (2008). The master curves were calculated at 90 °C and the spinning temperature, respectively.

Tensile measurements

The fibers breaking tenacity, breaking force, elongation at break and linear density were measured on an automatic single-fiber tester (Favigraph, Textechno, Germany) for conditioned and wet properties. Prior to the test, the fibers were conditioned over night at 20 °C and 65% relative humidity. The fiber count was 20 per sample. The test implemented a gauge length of 20 mm, 20 mm/min test speed and a sample pretention weight of 5.9 ± 1.2 mN/tex (according to DIN the 53816 standard). The Young's modulus of the fibers was derived from the elastic region in the stress strain curve based on the ASTM standard D2256/D2256.

Scanning electron microscope (SEM)

Cross-sectional images of the fibers were obtained via a Zeiss Sigma VP SEM with an acceleration voltage of 1.5 kV. The samples were prepared via sputter coating with Au prior to the imaging.

X-ray diffraction and birefringence

The regenerated cellulose fibers were first washed again with water before the X-ray diffraction (XRD) measurements. XRD data were analyzed via SmartLab (RIGAKU) instrument operated at 45 kV and 200 mA (λ = 1.5418 Å). Prior to the measurement, the fibers were cut into small shreds and pressed to form pellets. Using a sample holder with a transmission geometry, the powder diffraction data were collected in the continuous line scan mode with $\theta/2\theta$ geometry from 5° to 60° 2θ, available in Fig. S1 a. Azimuthal profiles of (020) diffraction peak were scanned with chi scan mode.

An air scattering profile without samples was collected under the same experimental condition and was subtracted from the intensity profiles of the samples. The subtracted data, illustrated in Fig. S1b, were smoothed using Savitzky-Golay filter with a window size of 29 and a polynomial order of 1. The smoothed data were corrected for inelastic scattering.

The background profile ($I_{bkg}(\theta)$) was estimated using a smoothing method applying Savitzky-Golay filter from 8° to 55° 2θ for each diffraction profile. Window size and polynomial order for the Savitzky-Golay filter were set to 201 (corresponding to 4° by 2θ) and 1, respectively. Iteration for the background estimation was repeated 50 times until there was no significant reduction in the background area. Then the crystallinity index (*CI*) was estimated using the ratio of the area of total intensity and of the above estimated background intensity from 9° to 50° 2θ:

$$CI = \frac{\int I(\theta)d\theta - \int I_{bkg}(\theta)d\theta}{\int I(\theta)d\theta} \quad (2)$$

The background corrected profiles in the range from 8° to 26° 2θ were fitted with four pseudo-Voigt functions for (1-10), (110), and (020) equatorial diffraction peaks, and a diffraction peak for meridian (002) peak as shown in Fig. S1 c. Latter meridian peak was added because a visible shoulder was present at 17.2° 2θ probably due to the preferential orientation originating from the fibrous morphology of the samples. The software lmfit was used for the fitting as shown. Scherrer equation was used to estimate the crystal widths (CW_{hkl}) of equatorial lattice of cellulose II as follows:

$$CW_{hkl} = \frac{K\lambda}{\beta_{hkl}\cos\theta} \quad (3)$$

where K = 0.90 is shape factor, λ is the X-ray wavelength, β_{hkl} is the full width at half maximum (FWHM) of the diffraction peak in radians and θ is the diffraction angle of the peak. Due to the significant overlap of diffraction peaks, the crystal width was reported by the average from three equatorial diffraction peaks. ESI Table S1 describes the crystal width of the fibers.

Herman's orientation parameter between cylindrical longitudinal direction and the crystallographic c-axis of unit cell was estimated from the azimuthal profile of (020) diffraction peak assuming cylindrical symmetry along the fiber as previously described (Yoshiharu et al. 1997).

The total orientation of the fibers was measured by the means of a polarized light microscope (Zeiss Axio Scope) equipped with a 5λ Berek compensator. The birefringence (Δn) was calculated by dividing the retardation of the polarized light by the fiber thickness. The total orientation (f_t) was determined by dividing the birefringence Δn by the maximum birefringence of cellulose (0.062) (Lenz et al. 1994). A factor $f_t = 1$ means the chains are perfectly aligned longitudinally, $f_t = 0$ means random orientation.

By knowing the total orientation f_t, the crystallinity (x_c) and the crystalline orientation (f_c), the amorphous orientation (f_a) could be calculated using the below equation

$$f_a = \frac{f_t - (x_c * f_c)}{(1 - x_c) * 0.91} \quad (4)$$

where 0.91 is the ratio of the amorphous and the crystalline densities of cellulose.

Results and discussion

All superbase-based ILs studied herein dissolved pulp cellulose readily, resulting in solutions with similar rheological properties. The importance of the rheological behavior for the spinnability in the dry-jet wet spinning process has been discussed in detail earlier (Hummel et al. 2016; Michud et al. 2015b). A defined balance between viscous fluidity and elastic behavior is a key parameter. High-throughput extrusion of the dope requires shear thinning upon shear stress in the spin capillary to avoid overly high pressures. The resulting filaments must then depict a certain elasticity to withstand the uniaxial stress exerted through the draw in the air gap before they immerge into the coagulation bath where they solidify (Nishiyama et al. 2019). Oscillatory shear measurements at various temperatures provided the complex viscosity and dynamic moduli for each cellulose-IL solution. As expected, they were all non-Newtonian fluids with strong shear thinning. At low angular frequency, the complex viscosity curves approached the Newtonian plateau. Through WLF time–temperature superposition, the data points could be shifted to even lower angular frequency than accessed during the measurement, making the Newtonian plateau even more visible (Fig. 1, left).

The Cross model was used to fit the complex viscosity and calculate the limiting value further referred to as the "zero shear" viscosity (η_0). However, this value would only correspond to the real (= dynamic) η_0 if the Cox–Merz rule is valid (i.e.,

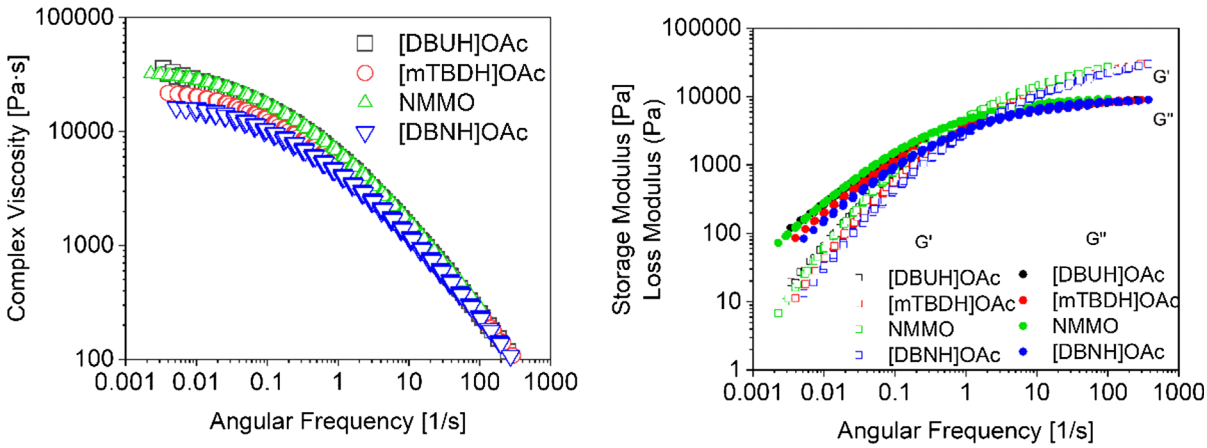

Fig. 1 Master curves of complex viscosity (left) and dynamic moduli (right) of the pulp solutions at temperature 90 °C

complex and dynamic viscosity as function of shear rate and angular frequency, respectively, superimpose perfectly). This has been confirmed by some authors (Haward et al. 2012), whereas others found pronounced differences in complex and dynamic viscosities (Chen et al. 2011; Lu et al. 2012). Using the master curve to calculate the η_0 value should be more accurate since the data set reaches further into the Newtonian plateau. However, we found that the difference between the limiting values calculated from the original data at the respective measurement temperature and those calculated through extrapolation of the master curve were statistically insignificant. Thus, η_0 values can also be calculated straight from the measurement data. Additional information of the η_0 values are available in the ESI Fig. S2.

NMMO and [DBNH]OAc are already known solvents in the lyocell technology. The respective cellulose solutions depict visco-elastic properties adequate for the dry-jet wet spinning (Fink et al. 2001; Hummel et al. 2016; Sixta et al. 2015). The rheological measurements of the dopes prepared with [mTBDH]OAc and [DBUH]OAc revealed similar properties. Figure 1 (left) shows the complex viscosity curves of the pulp solutions from the superbase ILs and NMMO at 90 °C. Both NMMO and [DBUH]OAc dopes express the highest η_0, while [mTBDH]OAc and [DBNH]OAc dopes are slightly lower. At higher angular frequency, all solutions reveal strong shear thinning until the curves virtually superimpose. Storage and loss moduli of the same solutions and temperature are shown in Fig. 1 (right). The differences between the solutions are even less pronounced than for the complex viscosity. As reported already earlier, the regions in which the storage modulus G' scales with ω^2 and G'' scales with ω were outside the measurement range, typical for highly concentrated cellulose solutions (Hummel et al. 2016).

The dynamic moduli also allowed for the calculation of the relaxation time spectrum of the pulp cellulose in the respective IL. Since pulp cellulose is not a monodisperse uniform polymer, each carbohydrate chain is characterized by an individual relaxation time. The resulting relaxation time spectrum can be directly correlated to the molecular weight distribution. Figure 2 (right) shows the relaxation time spectrum of the pulp in each ionic liquid.

H(lambda) is related to the number of molecules or components with a certain relaxation time (Ayad et al. 2001; Fulchiron et al. 1995; Meister and Kosan 2015). Besides differences in intensity of H(lambda)*-lambda, the relaxation time spectra of all spinnable solutions have a similar distribution. For comparison, the spectrum of the same pulp cellulose dissolved at 13 wt% in [emim]OAc was added. This particular solution was found non-spinnable under the dry-jet wet conditions applied to all other spin dopes (Hauru et al. 2016). The intensity is significantly reduced, and the maximum shifted to lower relaxation time values. This is in line with the observed reduced elastic and more viscose behavior of the [emim]OAc dope, leading to capillary breach in the air gap and impeding stable spinning (Ziabicki and Takserman-Krozer 1964a, b). A summary of the rheology data can be found in the ESI Table S2.

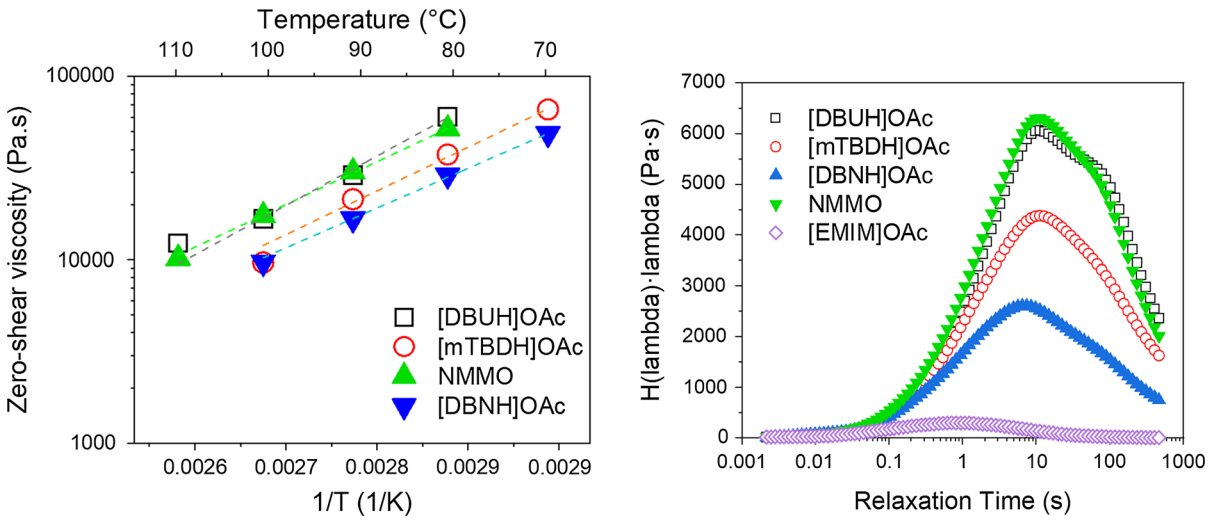

Fig. 2 Left: η_0 of the solutions over the temperature range. Right: Relaxation time spectra of the solutions at temperature of 90 °C

The temperature dependence of the η_0 is shown in the Arrhenius plot in Fig. 2 (left). The activation energy of flow (E_A) was calculated using the Arrhenius equation $\eta_0 = A^*\exp(E_A/RT)$, with R as the universal gas constant and the temperature (T) in K. It was noted earlier that ILs and their polymer solutions might not show a fully linear trend in the Arrhenius plot but rather depict a slightly convex evolution, which is more accurately represented by the Vogel-Fulcher-Tamman equation typically used for glass-forming liquids (Fröba et al. 2008). However, we and others found earlier that a simple Arrhenius fit is sufficiently accurate for a qualitative comparison of the different solutions (Gericke et al. 2009; Hummel et al. 2019). The activation energy of flow was in the range of 57–67 kJ/mol for all pulp solutions studied herein. This values are in line with previously reported activation energies for pulps with a similar DP in ionic liquid (40–70 kJ/mol) (Gericke et al. 2009) or NMMO solutions (40–90 kJ/mol) (Blachot et al. 1998; Gavillon and Budtova 2007).

In numerous earlier studies we have found that the dopes are spinnable at temperatures where the η_0 is in the range of 30 kPa.s and the cross-over point (COP) of the dynamic moduli occurs at 0.8–1.2 s^{-1} and around 4000 Pa (Hummel et al. 2016; Michud et al. 2015b; Sixta et al. 2015). The spinning temperature was then chosen accordingly so that above criteria were met. The angular frequency of the COP was 0.8 s^{-1} for [DBNH]OAc at 80 °C, 0.83 s^{-1} for [mTBD]OAc at 85 °C, 1.17 and 1.02 s^{-1} for NMMO and [DBUH]OAc at 95 °C, respectively. Although these temperature differences are small, they might have a notable impact on the overall process economics when scaled to commercial scale.

While NMMO and [DBNH]OAc have been established as excellent solvents for cellulose dry-jet wet spinning in numerous studies, good spinnability was also observed for pulp solutions in [mTBDH]OAc and [DBUH]OAc. Homogenous filaments were extruded, drawn in the air gap and regenerated in the coagulation bath. The DR of the filaments could be increased gradually to reach a maximum DR of 12, a value that yields fibers with a linear density of 1.2–1.35 dtex (using spinnerets with a capillary diameter of 100 µm). Throughout the spinning process, no systematic filament breach in the air gap or in the spin bath was noticed apart from a few filament breaks that are inevitable in a batch-type process. Fibers at various DRs were collected for subsequent analyses.

The structural properties of the regenerated fibers are characterized and quantified through various parameters. The total polymer orientation is accessible via birefringence measurements. The crystalline orientation is obtained through diffraction measurements while the amorphous orientation is derived from the crystalline and total orientation as discussed in the materials and methods section. In general, fibers with high crystallinity and crystalline orientation have pronounced strength values. Table 1 summarizes the

Table 1 Fiber birefringence measurements and structural analyses (XRD)

	DR	[DBUH]OAc	[mTBDH]OAc	NMMO	[DBNH]OAc
n	2	0.042	0.038	0.041	0.040
	5	0.042	0.043	0.041	0.043
	12	0.043	0.046	0.041	0.044
f_t	2	0.68	0.61	0.66	0.64
	5	0.68	0.69	0.66	0.69
	12	0.70	0.74	0.66	0.71
x_c	2	0.35	0.34	0.32	0.35
	5	0.36	0.36	0.33	0.35
	12	0.38	0.36	0.35	0.35
f_c	2	0.79	0.74	0.73	0.71
	5	0.80	0.80	0.79	0.86
	12	0.83	0.80	0.79	0.85
f_a	2	0.68	0.60	0.69	0.66
	5	0.67	0.68	0.65	0.66
	12	0.68	0.77	0.65	0.69

development of the birefringence and chain orientation parameters as a function of DR for the different solvents.

Interestingly, all fibers show a high total orientation (0.61–0.68) and crystallinity (0.32–0.35) even at a low DR of 2. Moreover, at the same DR, the birefringence value of the fibers is ca. 0.04, which is significantly higher than that of a regular viscose fiber (0.025) (Jiang et al. 2012). The increased axial orientation of the cellulose polymers is attributed to the high shear stress acting on the polymer chains during the draw in the air gap while cellulose is still in the dissolved state. A gradual increase in DR increased the total orientation of [mTBDH]OAc and [DBNH]OAc fibers. However, the effect was far less pronounced in the case of NMMO and [DBUH]OAc fibers. The crystalline orientation developed with higher draws for all solvents. It is noteworthy, that fibers spun from superbase-based ILs exhibited a higher total and crystalline orientation than that of NMMO at DR 12. On the other hand, the increase in DR had little influence on the crystallinity, which was on a high level already at low DR. This is in alignment with our previous findings for [DBNH]OAc fibers (Hummel et al. 2016). In a similar manner, the amorphous orientation was not affected by the higher DRs except for [mTBDH]OAc fibers, which showed an increase from 0.6 to 0.77.

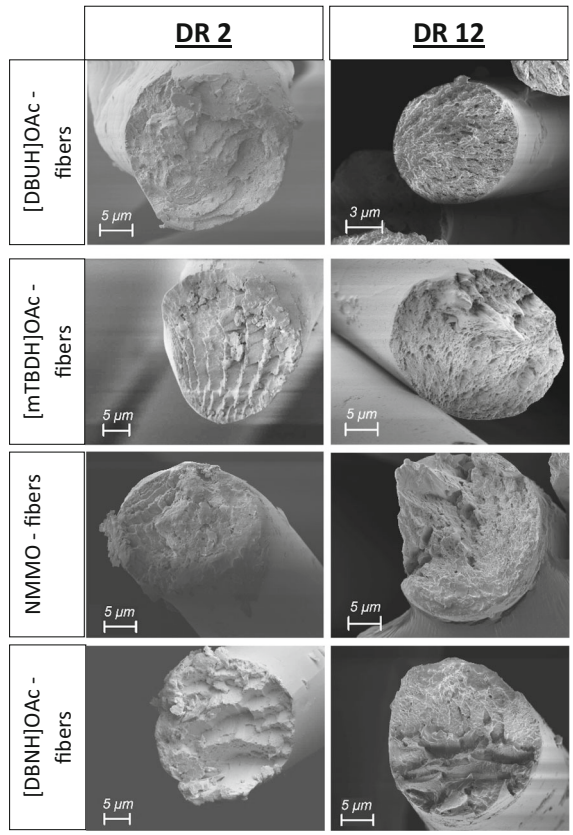

Fig. 3 SEM images of the fibers at DR 2 and 12

The morphology of the regenerated fibers at DR 2 and 12 was compared via scanning electron microscope (SEM) imaging, presented in Fig. 3.

At a lower DR, the cross-sectional images reveal more irregularities and non-homogeneities present in all the fibers. Polymer orientation is mostly induced by shear forces that occur during the extrusion of the dope through the spin capillaries. The shear strain, however, is only moderate due to the very low aspect ratio of the spin capillaries. At DR 12, the fibers possess a uniform circular cross section with a clearly fibrillar fiber body illustrating the improved orientation. As mentioned earlier, this is due to the predominant elongational polymer orientation in the air gap.

Figure 4 a displays the evolution of tenacity, elongation and linear density of the spun fibers as a function of the DR.

At a low DR of 3, all fibers exhibited linear density of 4.1–5.6 dtex and pronounced tenacities of 33.4–45.6 cN/tex. Compared to viscose fibers of DR 12, the ILs-based fibers possess higher tenacities even at such low draw (Hummel et al. 2016). Further increase in the take-up velocity only strengthened the filaments with minor decrease in the elongation. At the highest applied draw (12), the fibers titer was 1.2–1.3 dtex, ESI Fig. S3. As presented in Fig. 4 b, NMMO fibers showed the best elongation at break (12.4%) with a tensile strength of 46.5 cN/tex. On the other hand, [DBUH]OAc fibers expressed the highest strength (56.3 cN/tex) and a 9.8% elongation. [DBNH]OAc and [mTBDH]OAc fibers had somehow comparable tenacities of 49.5 and 49.9 cN/tex, respectively. However, higher elongation was depicted by the [DBNH]OAc fibers (12.2%) than [mTBDH]OAc fibers (9.8%), indicating that the latter fibers are slightly stiff. This is also shown in the modulus of elasticity of the [mTBDH]OAc and [DBUH]OAc fibers, where due to their lower elongation, they display the most pronounced modulus at DR 12 with 17.4 and 16.2 GPa, respectively. Contrarily, a lower modulus for NMMO (14.4 GPa) and [DBNH]OAc (13.9 GPa) fibers reflects higher elasticity. The elongation figures of the lyocell fibers discussed here are undoubtedly inferior when compared to the regular viscous ones. As explained earlier, this is due to the difference in the mechanism of regeneration of the wet spinning method, which enforces instant regeneration of the filaments once extruded. Hence, forming highly amorphous randomly distributed cellulose chains of low strength. Meanwhile, the fibers elongation can exceed 20% (Hummel et al. 2016).

It is well known that under wet conditions only cotton fibers preserve their strength and can even demonstrate wet-to-dry tenacities > 1. Viscose fibers, contrarily, exhibit considerably lower values of close to or even lower than 0.5 (Hummel et al. 2016).This is associated with the high amorphous orientation of the viscose fibers, which allows the accessibility of water to the inner core, thereby swelling it and cleaving the hydrogen bonds responsible for its strength (Hummel et al. 2016). However, the lyocell fibers, observed in Fig. 4 c, express improved wet-to-dry tenacities with the lowest of 0.85 and highest of 1. The intrinsically high crystallinity and crystalline orientation of the fibers seem to preserve their strength under the wet state.

Whilst all ionic liquids resulted in fibers of high quality, their potential for commercialization also depends on several other factors. [DBNH]OAc solutions could be spun at considerably lower temperatures than the only commercialized solvent NMMO monohydrate. This could offer energy and cost savings. However, the lyocell process requires almost complete solvent recycling to be commercially feasible. The recycling scheme for NMMO has been optimized over several decades and reached a recovery rate of $> 99\%$ (Rosenau et al. 2001). This is yet to be developed for ILs. The recovery rate depends on several crucial key points. One is the removal of the residual IL during the fiber washing step, since ILs can exhibit different affinities towards water and cellulose, which may vary the amount of required washing water and subsequently rise the costs because of extended washing lines. Another important feature is the hydrothermal stability of the solvent. Degradations has to be prevented to avoid detrimental solvent losses over the course of multiple cycles in a continuous process operation. For instance, DBN and its salts can undergo hydrolysis and subsequent irreversible amide formation that needs to be prevented or efficiently reversed (Parviainen et al. 2015). Recently, we successfully demonstrated that [mTBDH]OAc could be thermally recovered in the lyocell process without losing its dissolution power (Elsayed et al. 2020). This is due to the higher electron density of the sp^2-hybridized carbon of the guanidine that relatively protects the base against water nucleophilic reactions,

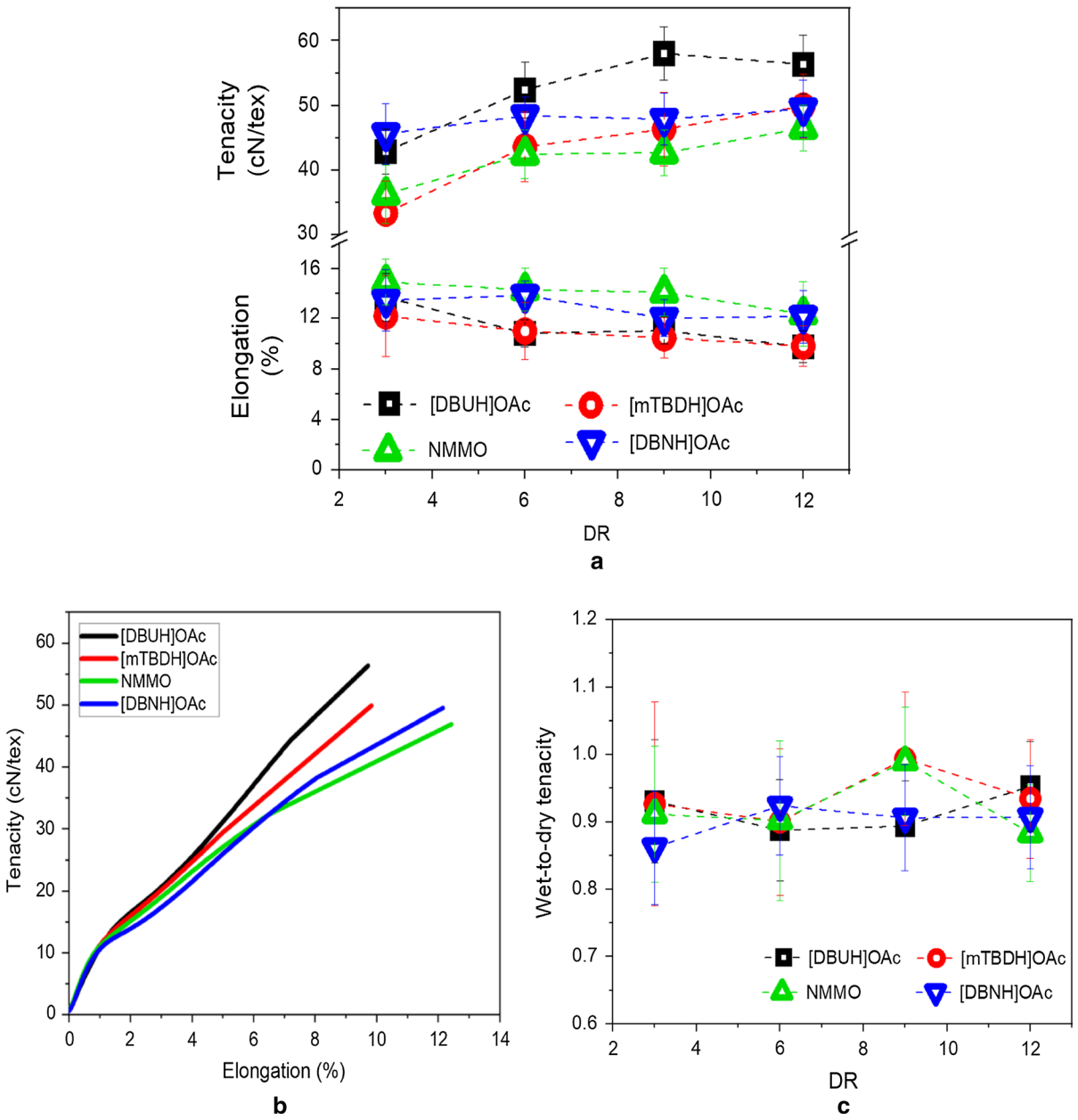

Fig. 4 Mechanical properties of the regenerated fibers. **a** Fibers conditioned tenacity, elongation and linear density at different DRs. **b** Fibers tenacity Vs. elongation at DR 12. **c** Fibers wet-to-dry tenacity at different DRs

whereas a fast relief in the ring strain of the amidines is dominant, producing the primary amines (Hyde et al. 2019). When [DBNH]OAc was subjected to the same recycling scheme, significant deviation in the solvent composition was detected that hindered cellulose dissolution in the following cycles (Elsayed et al. 2020).

Conclusion

The presented results show a high potential of IL solvents in the field of regenerated cellulose fibers. All solvents exhibited excellent cellulose dissolution power whilst producing a homogeneous solution adequate for the dry-jet wet spinning process. The rheological properties showed similar visco-elastic

behavior for all dopes suitable for dry-jet wet spinning. NMMO and [DBUH]OAc dopes possessed higher complex viscosity and dynamic moduli than the other solvents. Consequently, their spinning process demands a higher temperature than [mTBDH]OAc and [DBNH]OAc dopes. All fibers revealed both high crystallinity and crystalline orientation even at low DRs. Moreover, the tenacities of the superbase-based fibers were moderately above than those of NMMO fibers at DR 12. On the other hand, NMMO fibers had the best elongation that is similar to the [DBNH]OAc fibers. All fibers retained a high wet-to-dry tenacity, which is a unique property of the lyocell technology. In comparison to viscose fibers, the lyocell fibers exhibit higher crystallinity and orientation (higher strength) but lower elongation at break.

While the demonstrated fibers possess high quality, the selection and success of a new solvent for the lyocell process certainly depend on its recyclability. The proof-of-concept of successful and feasible recovery of the ILs is of significant importance for their commercialization. The long-term hydrothermal stability in a closed-loop operation process and the final recovery rate can only be evaluated once the size of the processing equipment exceeds a critical volume. Hence, pilot plant operations are needed to define the equilibrium of the possible degradations and side products from both the solvent and the solute.

Acknowledgments The authors would like to acknowledge the previous investigations by Kadvael Le Boulch in this topic. This work was possible by the internal funding of the Biofactory project in Aalto University.

Funding Open access funding provided by Aalto University.

Compliance with ethical standards

Conflict of interest The authors declare that they have no conflict of interest.

References

Ayad D, Carrot C, Guillet J (2001) Influence of the MWD of poly(vinylidene Fluoride) on its viscoelastic behaviour in the melt, part II: relaxation time spectra. Int J Polym Anal Charact 6:639–655. https://doi.org/10.1080/10236660108030874

Bentivoglio G, Roeder T, Fasching M, Buchberger M, Schottenberger H, Sixta H (2006) Cellulose processing with chloride-based ionic liquids. Lenzinger Berichte 86:154–161

Blachot J-F, Brunet N, Navard P, Cavaillé J-Y (1998) Rheological behavior of cellulose/monohydrate of n-methylmorpholine n-oxide solutions part 1: liquid state. Rheol Acta 37:107–114. https://doi.org/10.1007/s003970050096

Brandt A, Hallett JP, Leak DJ, Murphy RJ, Welton T (2010) The effect of the ionic liquid anion in the pretreatment of pine wood chips. Green Chem 12:672–679. https://doi.org/10.1039/b918787a

Brandt A, Grasvik J, Hallett JP, Welton T (2013) Deconstruction of lignocellulosic biomass with ionic liquids. Green Chem 15:550–583. https://doi.org/10.1039/c2gc36364j

Bredereck K, Hermanutz F (2005) Man-made cellulosics. Rev Prog Color Relat Top 35:59–75. https://doi.org/10.1111/j.1478-4408.2005.tb00160.x

Budtova T, Navard P (2016) Cellulose in NaOH–water based solvents: a review. Cellulose 23:5–55. https://doi.org/10.1007/s10570-015-0779-8

Buijtenhuijs FA, Abbas M, Witteveen AJ (1986) The degradation and stabilization of cellulose dissolved in N-methylmorpholine N-oxide (NMMO). Papier (Darmstadt) 40:615–619

Chen X, Zhang Y, Wang H, Wang S-W, Liang S, Colby RH (2011) Solution rheology of cellulose in 1-butyl-3-methyl imidazolium chloride. J Rheol (NY) 55:485–494. https://doi.org/10.1122/1.3553032

Clough MT, Geyer K, Hunt PA, Son S, Vagt U, Welton T (2015) Ionic liquids: not always innocent solvents for cellulose. Green Chem 17:231–243. https://doi.org/10.1039/C4GC01955E

Crowhurst L, Mawdsley PR, Perez-Arlandis JM, Salter PA, Welton T (2003) Solvent-solute interactions in ionic liquids. PCCP 5:2790–2794. https://doi.org/10.1039/B303095D

Doherty TV, Mora-Pale M, Foley SE, Linhardt RJ, Dordick JS (2010) Ionic liquid solvent properties as predictors of lignocellulose pretreatment efficacy. Green Chem 12:1967–1975. https://doi.org/10.1039/C0GC00206B

Ebner G, Schiehser S, Potthast A, Rosenau T (2008) Side reaction of cellulose with common 1-alkyl-3-methylimidazolium-based ionic liquids. Tetrahedron Lett 49:7322–7324. https://doi.org/10.1016/j.tetlet.2008.10.052

El Seoud OA, Koschella A, Fidale LC, Dorn S, Heinze T (2007) Applications of ionic liquids in carbohydrate chemistry: a window of opportunities. Biomacromol 8:2629–2647. https://doi.org/10.1021/bm070062i

Elsayed S, Hellsten S, Guizani C, Witos J, Rissanen M, Rantamäki AH, Varis P, Wiedmer SK, Sixta H (2020) Recycling of superbase-based ionic liquid solvents for the production of textile-grade regenerated cellulose fibers in the lyocell process. ACS Sustain Chem Eng. https://doi.org/10.1021/acssuschemeng.0c05330

Everaert G, Van Cauwenberghe L, De Rijcke M, Koelmans AA, Mees J, Vandegehuchte M, Janssen CR (2018) Risk assessment of microplastics in the ocean: modelling approach and first conclusions. Environ Pollut 242:1930–1938. https://doi.org/10.1016/j.envpol.2018.07.069

Fink HP, Weigel P, Purz HJ, Ganster J (2001) Structure formation of regenerated cellulose materials from NMMO-solutions. Prog Polym Sci 26:1473–1524. https://doi.org/10.1016/S0079-6700(01)00025-9

Fröba AP, Kremer H, Leipertz A (2008) Density, refractive index, interfacial tension, and viscosity of ionic liquids [EMIM][EtSO4], [EMIM][NTf2], [EMIM][N(CN)2], and [OMA][NTf2] in dependence on temperature at atmospheric pressure. J Phys Chem B 112:12420–12430. https://doi.org/10.1021/jp804319a

Fukaya Y, Sugimoto A, Ohno H (2006) Superior solubility of polysaccharides in low viscosity, polar, and halogen-free 1,3-dialkylimidazolium formates. Biomacromol 7:3295–3297. https://doi.org/10.1021/bm060327d

Fukaya Y, Hayashi K, Wada M, Ohno H (2008) Cellulose dissolution with polar ionic liquids under mild conditions: required factors for anions. Green Chem 10:44–46. https://doi.org/10.1039/B713289A

Fulchiron R, Michel A, Verney V, Roustant JC (1995) Correlations between relaxation time spectrum and melt spinning behavior of polypropylene. II: melt spinning simulation from relaxation time spectrum. Polym Eng Sci 35:518–527. https://doi.org/10.1002/pen.760350610

Gavillon R, Budtova T (2007) Kinetics of cellulose regeneration from cellulose – NaOH – water gels and comparison with cellulose – N-methylmorpholine-N-oxide – water solutions. Biomacromol 8:424–432. https://doi.org/10.1021/bm060376q

Gazit OM, Katz A (2012) Dialkylimidazolium ionic liquids hydrolyze cellulose under mild conditions. Chemsuschem 5:1542–1548. https://doi.org/10.1002/cssc.201100803

Gericke M, Schlufter K, Liebert T, Heinze T, Budtova T (2009) Rheological properties of cellulose/ionic liquid solutions: from dilute to concentrated states. Biomacromol 10:1188–1194. https://doi.org/10.1021/bm801430x

Goldstein MC, Goodwin DS (2013) Gooseneck barnacles (Lepas spp.) ingest microplastic debris in the North Pacific Subtropical Gyre. PeerJ 1:e184 https://doi.org/10.7717/peerj.184

Hansen CM, Björkman A (1998) The ultrastructure of wood from a solubility parameter point of view. Holzforschung 52:335–344. https://doi.org/10.1515/hfsg.1998.52.4.335

Hattori K, Cuculo JA, Hudson SM (2002) New solvents for cellulose: hydrazine/thiocyanate salt system. J Polym Sci, Part A: Polym Chem 40:601–611. https://doi.org/10.1002/pola.10135

Hattori K, Abe E, Yoshida T, Cuculo JA (2004) New solvents for cellulose. II. Ethylenediamine/thiocyanate salt system. Polym J 36:123–130. https://doi.org/10.1295/polymj.36.123

Hauru LKJ, Hummel M, King AWT, Kilpelainen I, Sixta H (2012) Role of solvent parameters in the regeneration of cellulose from ionic liquid solutions. Biomacromol 13:2896–2905. https://doi.org/10.1021/bm300912y

Hauru LKJ, Hummel M, Nieminen K, Michud A, Sixta H (2016) Cellulose regeneration and spinnability from ionic liquids. Soft Matter 12:1487–1495. https://doi.org/10.1039/c5sm02618k

Haward SJ, Sharma V, Butts CP, McKinley GH, Rahatekar SS (2012) Shear and extensional rheology of cellulose/ionic liquid solutions. Biomacromol 13:1688–1699. https://doi.org/10.1021/bm300407q

Heinze T, Dicke R, Koschella A, Kull AH, Klohr E-A, Koch W (2000) Effective preparation of cellulose derivatives in a new simple cellulose solvent. Macromol Chem Phys 201:627–631. https://doi.org/10.1002/(SICI)1521-3935(20000301)201:6%3c627:AID-MACP627%3e3.0.CO;2-Y

Horvath AL (2006) Solubility of structurally complicated materials: I. Wood. J Phys Chem Ref Data 35:77–92. https://doi.org/10.1063/1.2360606

Hummel M, Michud A, Tanttu M, Asaadi S, Ma Y, Hauru LKJ, Parviainen A, King AWT, Kilpeläinen I, Sixta H (2016) Ionic liquids for the production of man-made cellulosic fibers: opportunities and challenges. In: Rojas OJ (ed) Cellulose chemistry and properties: fibers, nanocelluloses and advanced materials. Springer, Cham, pp 133–168. https://doi.org/10.1007/12_2015_307

Hummel M, Michud A, Ma Y, Roselli A, Stepan A, Hellstén S, Asaadi S, Sixta H (2019) High-performance lignocellulosic fibers spun from ionic liquid solution. In: Rosenau T, Potthast A, Hell J (eds) Cellulose science and technology. Wiley, New Jersey, pp 341–370. https://doi.org/10.1002/9781119217619.ch14

Hyde AM, Calabria R, Arvary R, Wang X, Klapars A (2019) Investigating the underappreciated hydrolytic instability of 1,8-diazabicyclo[5.4.0]undec-7-ene and related unsaturated nitrogenous bases. Org Process Res Dev 23:1860–1871. https://doi.org/10.1021/acs.oprd.9b00187

Jiang G, Huang W, Li L, Wang X, Pang F, Zhang Y, Wang H (2012) Structure and properties of regenerated cellulose fibers from different technology processes. Carbohydr Polym 87:2012–2018. https://doi.org/10.1016/j.carbpol.2011.10.022

Jusner P, Aoki M, Potthast A, Rosenau T (2020) A cautionary note on "exothermic events" upon contact of carbodiimide coupling agents and the cellulose solvent N-methylmorpholine-N-oxide. Cellulose 27:7349–7359. https://doi.org/10.1007/s10570-020-03293-5

Kamida K, Okajima K, Matsui T, Kowsaka K (1984) Study on the solubility of cellulose in aqueous alkali solution by deuteration IR and 13C NMR. Polym J 16:857–866. https://doi.org/10.1295/polymj.16.857

Kamide K, Okajima K, Kowsaka K (1992) Dissolution of natural cellulose into aqueous alkali solution: role of super-

molecular structure of cellulose. Polym J 24:71–86. https://doi.org/10.1295/polymj.24.71
Köhler S, Heinze T (2007) New solvents for cellulose: dimethyl sulfoxide/ammonium fluorides. Macromol Biosci 7:307–314. https://doi.org/10.1002/mabi.200600197
Kosmulski M, Gustafsson J, Rosenholm JB (2004) Thermal stability of low temperature ionic liquids revisited. Thermochim Acta 412:47–53. https://doi.org/10.1016/j.tca.2003.08.022
Kuzmina O, Bhardwaj J, Vincent SR, Wanasekara ND, Kalossaka LM, Griffith J, Potthast A, Rahatekar S, Eichhorn SJ, Welton T (2017) Superbase ionic liquids for effective cellulose processing from dissolution to carbonisation. Green Chem 19:5949–5957. https://doi.org/10.1039/C7GC02671D
Laus G, Bentivoglio G, Schottenberger H, Kahlenberg V, Kopacka H, Röder T, Sixta H (2005) Ionic liquids: current developments, potential and drawbacks for industrial applications. Lenzinger Berichte 84:71–85
Lê HQ, Sixta H, Hummel M (2019) Ionic liquids and gamma-valerolactone as case studies for green solvents in the deconstruction and refining of biomass. Curr Opin Green Sustain Chem 18:20–24. https://doi.org/10.1016/j.cogsc.2018.11.009
Lenz J, Schurz J, Wrentschur E (1994) On the elongation mechanism of regenerated cellulose fibers. Holzforschung 48:72–76. https://doi.org/10.1515/hfsg.1994.48.s1.72
Liebert T (2010) Cellulose solvents - remarkable history, bright future. In: Liebert T, Heinze TJ, Edgar KJ (eds) Cellulose solvents: for analysis, shaping and chemical modification, vol 1033. ACS symposium series. American Chemical Society, Washington, pp 3–54
Lu F, Cheng B, Song J, Liang Y (2012) Rheological characterization of concentrated cellulose solutions in 1-allyl-3-methylimidazolium chloride. J Appl Polym Sci 124:3419–3425. https://doi.org/10.1002/app.35363
Ma Y, Hummel M, Maattanen M, Sarkilahti A, Harlin A, Sixta H (2016a) Upcycling of waste paper and cardboard to textiles. Green Chem 18:858–866. https://doi.org/10.1039/c5gc01679g
Ma Y, Hummel M, Sixta H (2016b) Effect of lignin concentration in birch kraft pulp on fibre spinning from ionic liquid solutions. In: American Chemical Society. ACS spring meeting, San Diego
Maeki-Arvela P, Anugwom I, Virtanen P, Sjoeholm R, Mikkola JP (2010) Dissolution of lignocellulosic materials and its constituents using ionic liquids—a review. Ind Crops Prod 32:175–201. https://doi.org/10.1016/j.indcrop.2010.04.005
Meine N, Benedito F, Rinaldi R (2010) Thermal stability of ionic liquids assessed by potentiometric titration. Green Chem 12:1711–1714. https://doi.org/10.1039/c0gc00091d
Meister F, Kosan B (2015) A tool box for characterization of pulps and cellulose dopes in Lyocell technology. Nord Pulp Pap Res J 30:112–120. https://doi.org/10.3183/npprj-2015-30-01-p112-120
Michud A, Hummel M, Haward S, Sixta H (2015a) Monitoring of cellulose depolymerization in 1-ethyl-3-methylimidazolium acetate by shear and elongational rheology. Carbohydr Polym 117:355–363. https://doi.org/10.1016/j.carbpol.2014.09.075
Michud A, Hummel M, Sixta H (2015b) Influence of molar mass distribution on the final properties of fibers regenerated from cellulose dissolved in ionic liquid by dry-jet wet spinning. Polym J 75:1–9. https://doi.org/10.1016/j.polymer.2015.08.017
Michud A, Hummel M, Sixta H (2016a) Influence of process parameters on the structure formation of man-made cellulosic fibers from ionic liquid solution. J Appl Polym Sci 133:177–185. https://doi.org/10.1002/app.43718
Michud A, Tanttu M, Asaadi S, Ma Y, Netti E, Kääriainen P, Persson A, Berntsson A, Hummel M, Sixta H (2016b) Ioncell-F: ionic liquid-based cellulosic textile fibres as alternative to viscose and Lyocell. Text Res J 86:543–552. https://doi.org/10.1177/0040517515591774
Nishiyama Y, Asaadi S, Ahvenainen P, Sixta H (2019) Water-induced crystallization and nano-scale spinodal decomposition of cellulose in NMMO and ionic liquid dope. Cellulose 26:281–289. https://doi.org/10.1007/s10570-018-2148-x
Parviainen A, King AWT, Mutikainen I, Hummel M, Selg C, Hauru LKJ, Sixta H, Kilpeläinen I (2013) Predicting cellulose solvating capabilities of acid-base conjugate ionic liquids. Chemsuschem 6:2161–2169. https://doi.org/10.1002/cssc.201300143
Parviainen A, Wahlström R, Liimatainen U, Liitiä T, Rovio S, Helminen JKJ, Hyväkkö U, King AWT, Suurnäkki A, Kilpeläinen I (2015) Sustainability of cellulose dissolution and regeneration in 1,5-diazabicyclo[4.3.0]non-5-enium acetate: a batch simulation of the IONCELL-F process. RSC Adv 5:69728–69737. https://doi.org/10.1039/C5RA12386K
Pinkert A, Marsh KN, Pang S, Staiger MP (2009) Ionic liquids and their interaction with cellulose. Chem Rev 109:6712–6728. https://doi.org/10.1021/cr9001947
Rinaldi R (2011) Instantaneous dissolution of cellulose in organic electrolyte solutions. Chem Commun (Cambridge, UK) 47:511–513. https://doi.org/10.1039/c0cc02421j
Rosenau T, Potthast A, Sixta H, Kosma P (2001) The chemistry of side reactions and byproduct formation in the system NMMO/cellulose (Lyocell process). Prog Polym Sci 26:1763–1837. https://doi.org/10.1016/S0079-6700(01)00023-5
Sammons RJ, Collier JR, Rials TG, Petrovan S (2008) Rheology of 1-butyl-3-methylimidazolium chloride cellulose solutions. I. Shear rheology. J Appl Polym Sci 110:1175–1181. https://doi.org/10.1002/app.28733
Singh S, Simmons BA (2013) Ionic liquid pretreatment: mechanism, performance, and challenges. In: Wyman CE (ed) Aqueous pretreatment of plant biomass for biological and chemical conversion to fuels and chemicals, pp 223–238. https://doi.org/10.1002/9780470975831.ch11
Sixta H, Michud A, Hauru L, Asaadi S, Ma Y, King A, Kilpeläinen I, Hummel M (2015) Ioncell-F: a high-strength regenerated cellulose fibre. Nord Pulp Pap Res J 30:43–57
Swatloski RP, Spear SK, Holbrey JD, Rogers RD (2002) Dissolution of cellulose with ionic liquids. JACS 124:4974–4975. https://doi.org/10.1021/ja025790m
The Fiber Year (2013) World survey on textiles and nonwovens, Issue 13
The Fiber Year (2019) World survey on textiles and nonwovens, Issue 19

Walden P (1914) Molecular weights and electrical conductivity of several fused salts. Bull Acad Imp Sci 1800:405–422

Wang H, Gurau G, Rogers RD (2012) Ionic liquid processing of cellulose. Chem Soc Rev 41:1519–1537. https://doi.org/10.1039/c2cs15311d

Welton T (1999) Room-temperature ionic liquids. Solvents for synthesis and catalysis. Chem Rev 99:2071–2083. https://doi.org/10.1021/cr980032t

Yamashiki T, Matsui T, Kowsaka K, Saitoh M, Okajima K, Kamide K (1992) New class of cellulose fiber spun from the novel solution of cellulose by wet spinning method. J Appl Polym Sci 44:691–698. https://doi.org/10.1002/app.1992.070440416

Yoshiharu N, Shigenori K, Masahisa W, Takeshi O (1997) Cellulose microcrystal film of high uniaxial orientation. Macromolecules 30(6395–6397):1. https://doi.org/10.1021/ma970503y

Ziabicki A, Takserman-Krozer R (1964a) Effect of rheological factors on the length of liquid threads. Colloid Polym Sci 199:9–13. https://doi.org/10.1007/bf01499686

Ziabicki A, Takserman-Krozer R (1964b) Mechanism of breakage of liquid threads. Colloid Polym Sci 198:60–65. https://doi.org/10.1007/bf01499455

Zweckmair T, Hettegger H, Abushammala H, Bacher M, Potthast A, Laborie M-P, Rosenau T (2015) On the mechanism of the unwanted acetylation of polysaccharides by 1,3-dialkylimidazolium acetate ionic liquids: part 1—analysis, acetylating agent, influence of water, and mechanistic considerations. Cellulose 22:3583–3596. https://doi.org/10.1007/s10570-015-0756-2